

www.acsabm.org Article

# Continuous, Nondestructive Detection of Microorganism Growth at **Buried Interfaces with Vascularized Polymers**

Brandon Dixon, Chenxi Sui, Anna Briley, Po-Chun Hsu, and Caitlin Howell\*



Cite This: ACS Appl. Bio Mater. 2023, 6, 519-528

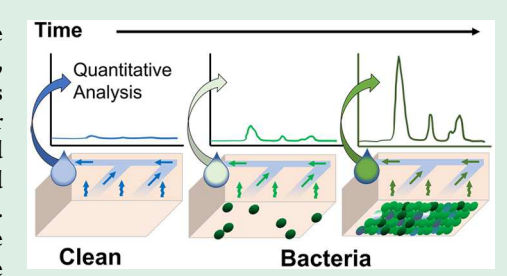


**ACCESS** I

Metrics & More

Article Recommendations

ABSTRACT: Evaluating surface bacterial growth at buried interfaces can be problematic due to the difficulties associated with obtaining samples. In this work, we present a new method to detect signals from microorganisms at buried interfaces that is nondestructive and can be conducted continuously. Inspired by vascular systems in nature that permit chemical communication between the surface and underlying tissues of an organism, we created a system in which an inert carrier fluid could be introduced into an empty vascular network embedded in a polymer matrix. When a microorganism layer was grown on top, small molecules produced by the growth process would diffuse down into the carrier fluid, which could then be collected and analyzed. We used this system to nondestructively detect signals from



a surface layer of Escherichia coli using conductivity, ultraviolet-visible (UV-vis) absorbance spectroscopy, and high-performance liquid chromatography (HPLC) for organic acids, methods that ranged in sensitivity, time-to-result, and cost. Carrier fluid from sample vascularized polymers with surface bacterial growth recorded significantly higher values in both conductivity and absorbance at 350 nm compared to controls with no bacteria after 24 h. HPLC analysis showed three clear peaks that varied between the samples with bacteria and the controls without. Tests tracking the change in signals over 48 h showed clear trends that matched the bacterial growth curves, demonstrating the system's ability to monitor changes over time. A 2D finite element model of the system closely matched the experimental results, confirming the predictability of the system. Finally, tests using clinically relevant Staphylococcus aureus and Pseudomonas aeruginosa yielded differences in conductivity, absorbance, and HPLC peak areas unique to each species. This work lays the foundation for the use of vascularized polymers as an adaptive system for the continuous, nondestructive detection of surface microorganisms at buried interfaces in both industry and medicine.

KEYWORDS: biofilms, biointerface, sensors, surface detection, bacteria

#### INTRODUCTION

The growth of bacteria on buried surfaces is problematic in a wide range of areas, including medical devices, 1-3 municipal water distribution networks, 4-8 and industrial processes. 9,10 In water distribution networks, in particular, it is known that water quality decreases as water travels through the underground distribution network due to the presence of bacteria on the interior surfaces of pipes.<sup>4–7</sup> However, detection of surface bacteria in buried systems such as these can be difficult, as the majority of the bacteria exists on the surface rather than in the liquid water phase. Although the use of materials which discourage bacterial growth can help reduce surface contamination,<sup>5,7</sup> it cannot eliminate it, which is of growing concern as the incidence of antibiotic resistance continues to rise around the world. 11-13 Methods which allow for regular monitoring of the bacterial load of buried interfaces are needed to provide an early warning system to reduce public health risks.

The current standard method for obtaining surface bacterial samples is through the use of swabs and contact plates.<sup>14</sup> Swabs and contact plates are considered nondestructive techniques, but results can vary due to heterogeneous swab materials and differences in user application pressure. 15-17 More aggressive methods like sonication and scraping can improve detection results; 3,18 however, conventional surface detection methods can be challenging to use when the surface to be evaluated cannot be easily accessed. For the detection of buried surfaces, sum-frequency vibrational spectroscopy (SFG) has been used. 19-22 However, this method relies on the ability of both visible and infrared light to penetrate through the substrate, 23,24 rendering it unsuitable for applications such as pipelines or implanted medical devices.

As they grow, microorganisms release numerous compounds that have the potential to be targeted for detection. <sup>25-30</sup> A study of the E. coli metabolome indicates a majority of the compounds released are amino acids.31 To detect the

Received: September 29, 2022 Accepted: December 22, 2022 Published: January 12, 2023





compounds produced by bacteria, conductivity has served as a common inexpensive method for monitoring the growth of bacteria as the production of charged metabolites and breakdown of large uncharged molecules from bacterial growth increase a solution's conductivity. 32,33 Advancements in UVvis absorbance spectroscopy have also allowed for the detection of organic compounds such as bacterial metabolites.<sup>34</sup> Additionally, compounds and the concentrations at which they are produced by bacteria differ between species. For example, the metabolites pyoverdine and pyocyanin are responsible for the distinct blue-green hue of P. aeruginosa. 35,36 By exploiting the differences in organic compounds, it is possible to identify bacterial species using advanced detection methods such as gas chromatography-mass spectrometry.<sup>2</sup> A surface detection system for buried interfaces would need to allow for bacterial-specific compounds to diffuse from the surface and be collected for later analysis.

In nature, both plant and animal systems use vascular networks to detect bacteria at surfaces.<sup>37–39</sup> Diffusion allows for signal molecules to be transferred into the vascular network. Long-range transport of the signal molecules throughout the system then allows for the appropriate detection and response mechanisms for survival. To create a vascular network in a polymer matrix, direct-ink-writing (DIW), a 3D printing process, has been developed and used for a variety of biomedical applications. 40-42 In particular, a subsection of DIW known as fugitive ink printing has allowed for the fabrication of embedded vascular systems in polymers. 43 By filling channels with fluids for their desired characteristics, vascularized polymers have been promising in antifouling, 44 self-healing, 45 spatial control, 46 and heat exchange applications. 47,48 Furthermore, bacterial signaling has been observed and controlled through flow-assembled chitosan membranes in microfluidic systems. 49,50 Vascularized polymers can now be fabricated and used for a variety of applications.

In this work, we develop and test a method to detect bacteria at buried interfaces that is nondestructive and continuous. Inspired by vascular systems in nature that permit chemical communication between the surface and underlying tissues of an organism, we detect chemical signals diffusing from surface E. coli in channels filled with an inert carrier fluid embedded in a polymer matrix. We use conductivity, UV-vis absorbance spectroscopy, and HPLC-methods that ranged in sensitivity and cost—to detect differences between vascularized polymer samples with bacteria and those without. Extracting and refilling the vascular channels with new carrier fluid allowed us to continuously monitor bacterial growth over a 48-h period, while modeling the system using a 2D finite element approach permitted us to predict the changes over time with high accuracy. Finally, we test two other species of bacteria, S. aureus and P. aeruginosa, and demonstrate that it is possible to distinguish one species from the other. This work lays the foundation for the use of vascularized polymers as an adaptive system for the continuous, nondestructive detection of surface bacteria along with multiple methods for analysis.

#### EXPERIMENTAL SECTION

Materials. Difco Bacto agar, Miller's Luria—Bertani (LB) agar, and Miller's LB broth were acquired from Fisher Scientific. Pluronic F127 powder was sourced from Sigma-Aldrich. Phosphate-buffered saline (PBS) at a 10× concentration was purchased from Teknova. All

solutions were created with deionized water and sterilized via autoclaving at 121  $^{\circ}\mathrm{C}$  for 60 min.

Vascularized Polymer Fabrication. Vascular channels were designed in SolidWorks and converted to G-code commands using Slic3r slicing software. Difco Bacto agar (1.5%) cooled to touch was poured in a 100 × 100 × 15 mm square polystyrene Petri dish. After cooling overnight, vascular network channels were printed using 30% w/v Pluronic F127 fugitive ink through a 15-gauge blunt tipped needle directly on the agar using a Hyrel System 30 M printer equipped with a VOL-25 extruder head heated to 30 °C. Once the channels had been printed, 20 g of 1.5% Difco Bacto agar was poured directly over the solid agar with channels and allowed to cool overnight. A 15 g aliquot of 4% Miller's LB agar cooled to touch was poured over the agar/channel system and again cooled overnight. Inlet and outlet holes were melted through the bottom of the Petri dish using a heated 15-guage blunt tip needle. Channels were evacuated using a pipet to remove the Pluronic F127. Channels were washed with deionized water twice and then filled with 1× PBS as the carrier fluid. PBS was chosen for this role as its salt content minimized immediate absorbance of the fluid into the agar matrix materials.

**Bacterial Cultures.** Initial surface detection and continuous detection tests were conducted using the bacterial strain *Escherichia coli* K12 W3110. For testing clinically relevant strains, *Staphylococcus aureus* SC01 and *Pseudomonas aeruginosa* PA01 wild type were used. All strains were stored in stock cultures at  $-80\,^{\circ}$ C. For experiments, streak plates were created on 4.0% LB agar, and liquid cultures were prepared via inoculation with 2–3 isolated colonies into test tubes containing 5 mL of LB broth at 37 °C for 24 h. An optical density (OD) of 0.08–0.10 au at 600 nm was achieved by diluting the sample with blank LB broth.

**Growth Curve Measurements.** Intensity measurements to track the growth of the bacteria on the agar surface were obtained using the iBright imaging system model FL1500. Images were taken with the colony no emission channel and smart exposure time of 36 ms. ImageJ was used to obtain intensity values for regions of interest bounded with rectangles.

**Conductivity Measurements.** Conductivity measurements were obtained using the Mettler Toledo FiveEasy conductivity meter and Inlab 751–4 mm probe. Measurements were recorded using the automatic measurement feature that waited for the sample and probe to reach equilibrium before displaying the reading.

**Absorbance Measurements.** Absorbance measurements were recorded using a Thermo Scientific Genesys 150 UV—visible spectrophotometer at 350 nm following organic matter wavelength parameters in water quality testing.<sup>34</sup> Fireflysci Sub-Micro cuvettes were implemented to allow absorbance readings of small volumes.

High-Performance Liquid Chromatography. HPLC analysis was carried out using a Shimadzu Prominence system equipped with a Bio-Rad Aminex HPX-87H column. UV—visible detection was conducted with the Shimadzu SPD-20AV detection unit at 254 nm. The mobile phase was 5 mM sulfuric acid with a flow rate of 0.6 mL/min, and the column oven temperature was set to 60 °C. All controls and samples were diluted 1:2 with Milli-Q water [resistivity 18.2 MΩ-cm @ 25 °C; total organic carbon (TOC)  $\leq$  5 ppb] before analysis.

**Surface** *E. coli* **Detection.** Vascularized polymers were filled with 1× PBS via the inlet and outlet holes. Inlet and outlet holes were sealed with vacuum grease and covered over with tape. Initial conductivity, absorbance, and HPLC analysis values were recorded using 1× PBS. A diluted *E. coli* liquid culture was applied to the surface of samples using a sterile cotton tip applicator. To create a uniform bacterial lawn, the entire surface was swabbed in a side-to-side motion, rotated 60°, and then reswabbed for a total of 3 passes. Controls were swabbed in the same manner with blank LB broth. Vascularized polymers were incubated at 37 °C. After 24 h of incubation, carrier fluid within the channels was evacuated and analyzed.

**Bacterial Growth Curve.** The bacterial growth curve for the system was generated by applying a diluted *E. coli* liquid culture to the surface of 4% LB agar plates. Plates were incubated at 37 °C. At multiple time points, plates were removed from incubation and

imaged using the iBright imaging system with the colony no emission channel and smart exposure time of 36 ms.

Continuous Detection. Vascularized polymers plates were prepared as described above. Throughout the 48-h growth period, vascularized polymers were removed from incubation at defined time points, and the carrier fluid with the channels was evacuated and analyzed. Channels were immediately refilled with fresh 1× PBS.

S. aureus and P. aeruginosa Detection. Vascularized polymer plates were prepared as described above for E. coli. The plates were incubated for 24 h at 37 °C before collection and analysis of the

Finite Element Simulation. The finite element simulation was conducted in COMSOL using the Transport of Diluted Species module to simulate the diffusion of chemical species within the system. The governing equation of the physical field is given by

$$\frac{\partial c}{\partial t} + \nabla \cdot J + \mathbf{u} \cdot \nabla c = R$$

$$I = -D\nabla c$$

where c is the local concentration of the species; R is the total rate expression; J is the flux; and D is the diffusivity. The velocity field of the liquid, u, is neglected because the convective flow in agar is minimal.

For the production model, we set the inward flux of the species on the top surface of the agar, expressed as

$$J = pX_{c} - ac$$

where p is the maximum production rate;  $X_c$  is the cell concentration (interpolated from the experiment results); and a is a degradation constant to account for the decrease of the production rate.

For the utilization model, we assumed that the bacterial cells on the top surface of agar consume nutrients, expressed as

$$J = \frac{-ckX_{\rm c}}{c + K_{\rm s}}$$

where  $K_s$  is the Monod half-velocity coefficient and k is the maximum utilization rate.52

To match the experimental conditions more accurately, the simulation was conducted in batches. In each batch, the concentration of the carrier fluid in the channel was reset to zero, while the initial concentrations in the agar were kept the same as at the end of the previous batch.

Statistical Analysis. Averages and standard deviations were calculated in Microsoft Excel using experimental data. Data were normalized by subtracting the control value average from sample values. To evaluate statistical significance, an assessment of normality and t tests were conducted in RStudio. An asterisk ranking system was implemented in figures to represent the p values with n.s., \*, \*\*, and \*\*\* corresponding to p > 0.05, p < 0.05, p < 0.01, and p < 0.001, respectively.

## RESULTS AND DISCUSSION

System Design and Overview. To create a synthetic vascular network, we used fugitive ink 3D printing in an agar polymer matrix. The model used for vascular channel design and the channel location within the vascularized polymers are depicted in Figure 1A. An image of a vascularized polymer used for testing is displayed in Figure 1B. Bacteria were grown on the underside of the polymer to create a buried interface, while inlet and outlet holes were created on the upper surface to allow for the carrier fluid to be filled and evacuated from the polymer channels.

As bacteria grew and synthesized compounds, the compounds diffused from the surface into the embedded channels within the polymer matrix via concentration gradients (Figure 1C). As time progressed, the bacterial-specific

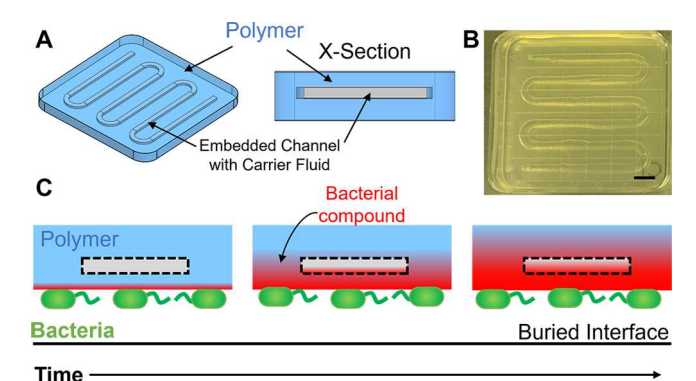


Figure 1. (A) 3D model of vascular channel designed and a crosssection highlighting the embedded channel location. (B) Photo of a vascularized polymer system after the fabrication process. Scale bar 1 cm. (C) Schematic of the system cross-section with bacteria-releasing compounds from the buried interface which diffuse into the channel network filled with the carrier fluid over time.

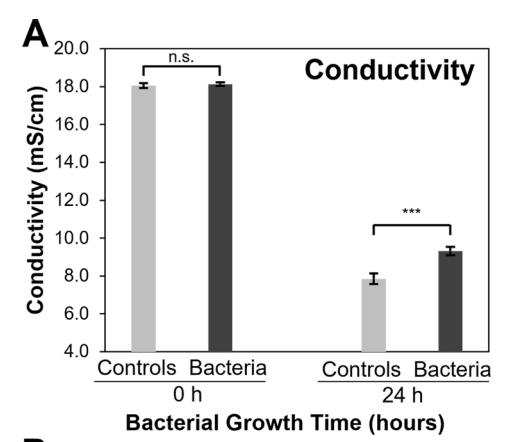
compounds accumulated in the carrier fluid within the channels, which were then evacuated for analysis.

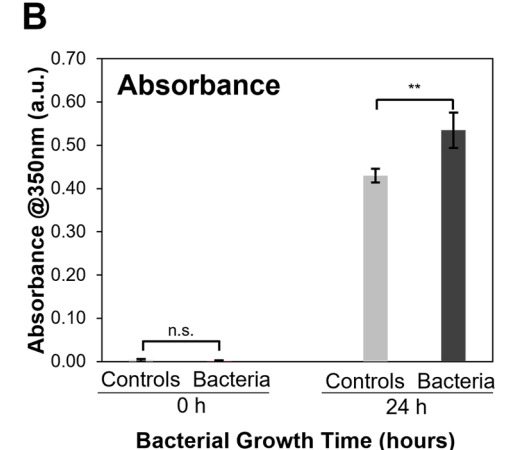
Nondestructive Detection of Surface Ecoli. E. coli was applied to the surface of a sample of vascularized polymers and compared against control vascularized polymers that lacked surface bacterial growth. Controls with no bacteria rather than dead bacteria were chosen to better represent a surface in which the desired state was bacteria-free, for example, a medical implant or drinking water pipeline. Multiple analysis methods were used to evaluate the carrier fluid from samples and controls (Figure 2). Conductivity was chosen due to its low cost and rapid time-to-result; UV-vis absorbance spectroscopy was used as it is a widely accessible technique and also returns information quickly; and HPLC was selected as it is more selective and sensitive than either conductivity or UV-vis analysis, despite having a higher cost and requiring more sample preparation time. The goal with these three analysis methods was to demonstrate the potential for vascularized polymer detection for both general (e.g., presence/absence, extent of growth) and specific (e.g., compound consumption and production, species detection) analysis.

Figure 2A shows the differences in conductivity between uninoculated controls and samples with surface E. coli. Time 0 values were obtained by measuring the carrier fluid before introduction into the vascular channels; as expected, there was no significant difference (p = 0.3860) between the samples. The high initial values were likely a result of the entirety of the salt component of the PBS carrier fluid contributing to the conductivity. After 24 h, the conductivity value for both carrier fluid from samples with surface E. coli and uninoculated controls dropped, likely due to the absorbance of some of the salts in the carrier fluid into the polymer matrix. Nevertheless, a significantly higher conductivity was observed from bacteriacontaining samples (9.32  $\pm$  0.22 mS/cm) compared to controls (7.86  $\pm$  0.29 mS/cm, p = 0.0003). The increase in carrier fluid conductivity was likely the result of charged molecules created during bacterial growth and metabolism that diffused from the surface into the carrier fluid. 32,33

Absorbance measurements at 350 nm for samples and controls are shown in Figure 2B. As for the conductivity measurements, there was no significant difference (p = 0.4810) between carrier fluid intended for the samples and controls

ACS Applied Bio Materials www.acsabm.org Article





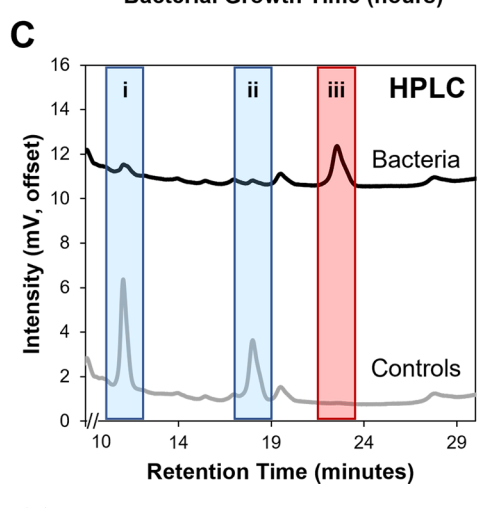


**Figure 2.** (A) Conductivity measurements of the carrier liquid within vascularized polymers with no bacteria at the surface (controls, n = 4) or with *E. coli* actively growing on the surface (bacteria, n = 5) after 0 and 24 h of growth. (B) Absorbance measurements from the samples shown in part (A). (C) HPLC chromatogram overlay with offset comparing the carrier fluid taken from vascularized polymers either with bacteria or without (controls) after 24 h of bacterial growth. Notable peaks are marked as i, ii, and iii. \*\*\* indicates P < 0.001; \*\* indicates P < 0.01; and n.s. indicates no significance.

before the experiment was conducted. After 24 h of bacterial growth, a significant increase in absorbance (p = 0.0026) was observed in samples (0.535  $\pm$  0.041 au) compared to controls (0.430  $\pm$  0.016 au). Organic matter is known to absorb at 350 nm, and this range is extensively used in water quality analysis.<sup>34</sup> The compounds being detected here are likely a mix of proteins, sugars, lipids, and other carbon-containing

compounds. As the major component of the LB carbon source, tryptone, does not show an absorbance peak at 350 nm, <sup>53</sup> it is logical that the growth of *E. coli* on the surface is producing more compounds which do absorb in this range which are diffusing down into the carrier fluid and being detected in our analysis.

Representative examples of the HPLC chromatograms obtained from the carrier fluid collected from E. coli-colonized samples and uninoculated controls after 24 h are displayed offset in Figure 2C. Three peaks of interest were observed in these spectra, appearing at retention times of 11.0 min (Peak i), 18.0 min (Peak ii), and 22.5 min (Peak iii). Peak i was observed to have a substantial area (135559 ± 25497 mV·min) in carrier fluid collected from uninoculated controls, while fluid from bacteria-colonized samples showed a notably smaller peak area (14765 ± 1554 mV·min) after 24 h. Similarly, Peak ii showed a larger area in fluid from controls (98188  $\pm$  4248 mV· min) than bacteria-containing samples (2335 ± 2703 mV· min). The decreases in both Peaks i and ii in E. coli-colonized samples compared to controls may be due to UV-active compounds in the LB media such as a tryptone, which is known to have an absorbance peak at 264 nm, close to the 254 nm detected here.<sup>53</sup> As the bacteria consume this food source or other compounds present, there is subsequently less available to diffuse into the carrier fluid in the channels below, resulting in a decreased peak. The final peak in the chromatograms, Peak iii, was not present in the carrier fluid controls but very clear in the fluid from the *E. coli* samples with a peak area of 92613 ± 8698 mV·min. The appearance of Peak iii in the samples containing surface E. coli suggests that this is a UV-active compound being produced by the bacteria. As E. coli growing on LB produce a very large number of compounds during their growth, 54,55 exact identification of this compound or group of compounds is outside the scope of this work; nevertheless, these results demonstrate the promise of using vascularized polymers to detect both general and more specific bacterial signals.

**Continuous Detection of Surface** *E.coli*. Once the feasibility of bacterial detection was established, we designed experiments to demonstrate the use of the vascularized polymer system to track changes in the *E. coli*-colonized surfaces over time. Carrier fluid was extracted and refilled in vascularized polymers multiple times throughout a 48-h growth period. Analysis of the carrier fluid at five different time points is shown in Figure 3. The gray shading behind each curve shows the experimentally determined growth curve for comparison, with the lag phase occurring between 0 and 4 h, the exponential phase from 4 to 12 h, and the stationary phase beginning at 12 h. The light intensity method used to obtain this curve could not distinguish between live and dead cells; therefore, the death phase may also be occurring between the 12 and 48 h time points.

Figure 3A shows the normalized conductivity measurements with the growth curve behind in gray shading. It is important to note that the residence time the carrier fluid spent in the vascularized channels collecting signals differs between data points. For example, at the 8 h measurement, the carrier fluid had resided for 4 h within the vascular channels (from 4 h to 8 h), while at the 24 h time point it had 12 h of collection time (from 12 h to 24 h). For the 48-h data point, the carrier fluid would have remained in the system for an entire 24 h to absorb bacterial-specific compounds from the surface. The difference

**ACS Applied Bio Materials** 

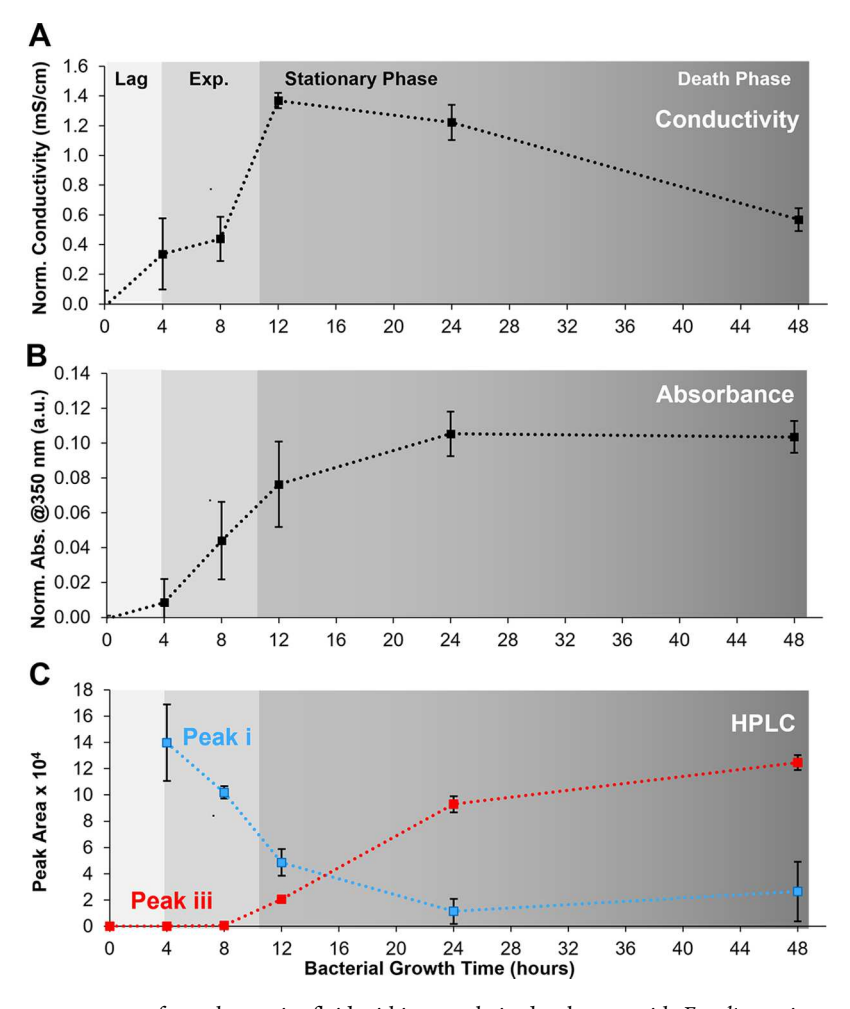


Figure 3. (A) Conductivity measurements from the carrier fluid within vascularized polymers with E. coli growing on the surface, normalized to uninoculated controls, n = 5, over a 48-h time period. The experimentally determined growth stage of the bacteria is indicated by the shade of the gray background. (B) Absorbance measurements for the same carrier fluid shown in (A), normalized to the uninoculated controls. (C) HPLC analysis of the same carrier fluid analyzed in (A) and (B): change in areas for the HPLC peaks at 11.0 min (Peak i) and 22.5 min (Peak iii) over the 48-h time period.

in residence time in the channels must therefore be taken into account when interpreting the results.

Throughout the continuous detection tests, the conductivity followed a trend similar to the growth curve: initial conductivity readings appeared to remain relatively stagnant from the 4 to 8 h mark; an increase in conductivity was then observed from 8 to 12 h with mark with a peak value of 1.37  $\pm$ 0.050 mS/cm; and then from the 12 to 24 h, normalized conductivity decreased to 1.22  $\pm$  0.118 mS/cm and further dropped to 0.568  $\pm$  0.076 mS/cm at the 48-h time period. A similar trend of increased conductivity during the exponential growth phase and a decrease in conductivity during the death phase were observed by Pavlova et al.<sup>32</sup> The gradual slowing and cessation of metabolite production during the death phase is likely the cause of this observation. Pavolova et al. also noted that conductivity of the E. coli culture was a highly sensitive tool to detect the state of microbial growth. Here, the clear change in conductivity at each growth stage, particularly the well-defined decrease in signal at 48 h, supports that conclusion.

The normalized absorbance recordings of the carrier fluid from the continuous detection test are shown in Figure 3B. Absorbance values remained relatively stagnant from 0 to 4 h. Similar to Figure 3A, absorbance sharply increased from 4 to

12 h. Peak absorbance occurred at 24 h of surface bacterial growth (0.105  $\pm$  0.013 au). A similar trend was exhibited in the normalized absorbance measurements. From the 24-h time point to the 48-h time point, absorbance values appeared to remain mostly steady. This may be due to the contribution of cellular breakdown products to the overall signal as the *E. coli* gradually enter the death phase.

Changes in HPLC peak areas over time are shown in Figure 3C. The two most prominent peaks, Peak i at 11.0 min and Peak iii at 22.5 min, are shown in blue and red, respectively. Data at the 0-h time point were not included as there was not sufficient time for diffusion from the surface to channels for analysis. Peak i decreased over time with the largest area measured initially at 4 h (139701 ± 29029 mV·min), followed by a decrease to 11345  $\pm$  9638 mV·min at 24 h, followed by a slight increase to 26459 ± 22701 mV·min at 48 h. In contrast, Peak iii was not detectable until 8 h of surface bacterial growth, at which the peak area increased to 639 ± 584 mV·min. After this time point, the peak continually increased to achieve a maximum peak area of 124715 ± 5674 mV·min at 48 h. Together, these results demonstrate that it is possible to continuously and nondestructively monitor the growth of E. coli at a buried interface using an embedded vascular network.

**ACS Applied Bio Materials** 

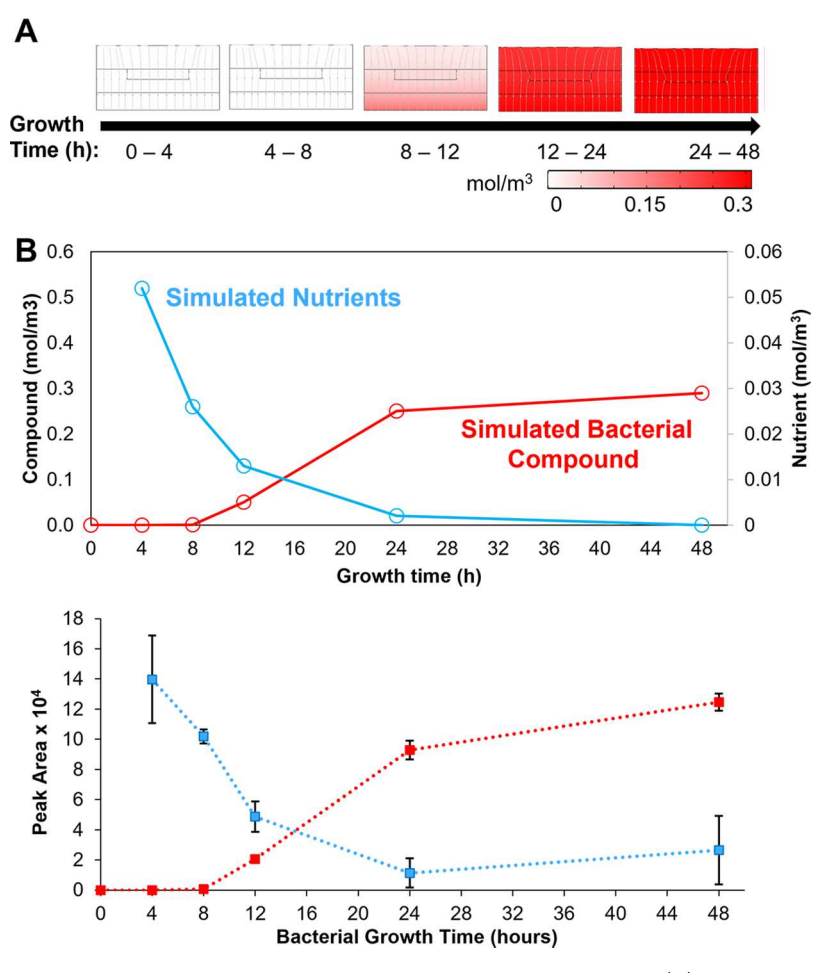


Figure 4. Finite element simulation of the bacteria's production and utilization of compounds. (A) Distribution of the bacterial compound concentration in the device at the end of each measurement period, showing that the products gradually diffused into the agar from the bottom. (B) The concentration of both the nutrients and the simulated bacterial compound as a function of time (above) and the experimental HPLC data for comparison (below).

**Finite Element Simulation.** As previously mentioned, bacteria produce thousands of low-molecular-weight compounds as part of their normal growth, <sup>54,55</sup> making it difficult to identify the exact compounds being measured at this time. Nevertheless, we wished to verify that the compounds we were detecting behaved in a way that was consistent with known bacterial production and consumption rates and could be predicted using equations established specifically for these parameters.

To model our system, we built a 2D simulation of our vascularized polymers, consisting of an upper layer of lowdensity agar (2.3 mm), a central layer (2.3 mm) containing a fluid-filled channel 6 × 1 mm wide, and finally a bottom layer of high-density agar (1.7 mm) containing diffusible "nutrients" throughout. The bottom layer was also set such that a "bacterial compound" would diffuse from the surface toward the channel (Figure 4A). As in our experimental system, the model was allowed to run for a defined number of hours before it was stopped and the concentration in the center channel measured. At this point the system reset with a concentration of zero in the channel, mimicking our extraction of the carrier fluid and refilling of the channel with fresh fluid. The governing equations used were adapted from previous work developing quantitative models for bacterial substrate utilization<sup>52</sup> and the production of low-molecular-weight compounds. 51 The results from finite element simulation for both nutrients and a

bacterial compound are shown in Figure 4B. The resulting curves for both matched very closely with the experimental results for HPLC analysis of fluid from *E. coli*-colonized surfaces shown in Figure 3C. The curve for the simulated nutrients showed a steep drop in concentration nearly identical with what was observed for Peak i; however, in the simulation the concentration reached zero at 48 h, while in our experiment the value showed a slight increase relative to 24 h. The simulated bacterial compound also showed a curve similar to Peak iii, with values for 0, 4, and 8 h at or near zero, followed by a jump at 12 h. There was again a difference between the experiment and model at 48 h, though the values for the model increased less over this final measurement period than the values in the experiment.

It is important to note that the while the simulation results match well with the HPLC data they do not follow the same trends as the conductivity and absorbance measurements. This is likely due to the fact that the conductivity and absorbance measurements detect several compounds, each with their own diffusion rates. The HPLC results, however, are separated out by compound, simplifying the system to the point where it can be accurately modeled. Nevertheless, our results confirm that the compounds that we are measuring in our experiment behave according to known quantitative models of bacterial nutrient utilization and compound production. This supports our hypothesis that we are accurately measuring compounds

ACS Applied Bio Materials

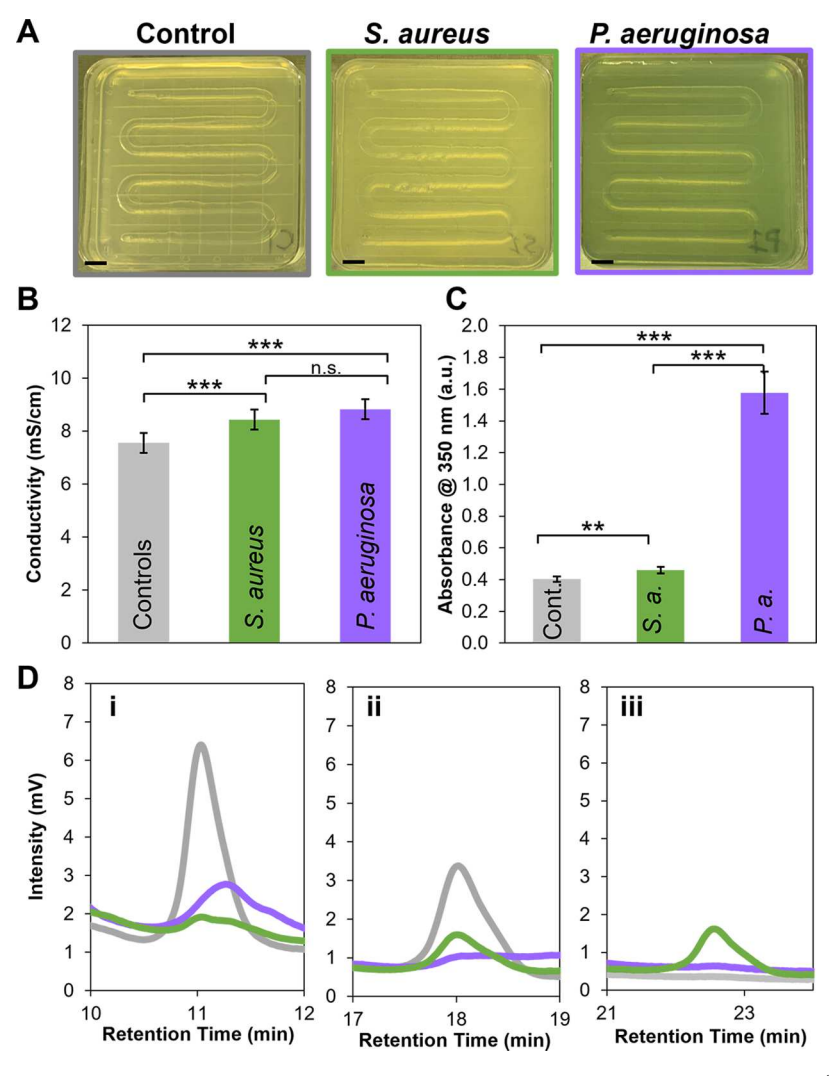


**Figure 5.** (A) Images of the vascularized polymer systems showing the differences in color between the treatments. (B) Normalized conductivity measurements from samples (n = 4). Exact data values are given in the text. (C) Normalized absorbance measurements from samples (n = 4). (D) Three HPLC peaks from carrier fluid obtained from control (gray), *S. aureus* (green), and *P. aeruginosa* (purple) samples. Designations of (i), (ii), and (iii) indicate Peaks i, ii, and iii as identified in Figure 2C.

associated with bacterial growth using our vascularized polymer system and, furthermore, that our system can be quantitatively modeled for future applications in surface sensing.

**Detection of Other Bacterial Species.** Once it was established that continuous and nondestructive monitoring of *E. coli* could be successfully accomplished, tests were conducted on other clinically relevant bacterial species. *S. aureus* and *P. aeruginosa* were selected for testing as they are common pathogens associated with infections in hospital settings. Additionally, *P. aeruginosa* is additionally known for its biofilm formation abilities and presence in water distribution networks. 4,7,8,56

A visible difference in color was clear among the vascularized polymers without surface bacteria (controls), those with *S. aureus*, and those with *P. aeruginosa* surface growth (Figure 5A). Samples with *P. aeruginosa* displayed a blue-green hue most likely from the metabolites, pyoverdine and pyocyanin, that resulted in its distinct coloration, 35,36 whereas samples colonized by *S. aureus* appeared to be the same hue as the control with a fuzzy lawn of surface bacterial growth.

The conductivity of the carrier fluids in vascularized polymers was measured after 24 h of surface bacterial growth (Figure 5B). Samples with P. aeruginosa surface growth recorded the highest conductivity value (8.823 ± 0.275 mS/ cm), significantly higher than the controls (p = 0.0009). Samples colonized by S. aureus exhibited a greater conductivity  $(8.428 \pm 0.186 \text{ mS/cm})$  than the controls  $(7.551 \pm 0.120 \text{ mS/cm})$ cm) and were statistically significant (p = 0.0005). Carrier fluid conductivity measurements were not statistically different between samples with P. aeruginosa surface growth and samples with S. aureus surface growth (p = 0.0604). As with the samples colonized by E. coli, the increase in carrier fluid conductivity of sample vascularized polymers was most likely the result of a charged bacterial compound from general bacterial metabolic activity diffusing from the surface into the channels. 32,33

Absorbance measurements of the carrier fluid at 350 nm after 24 h were also measured (Figure 5C). *P. aeruginosa* exhibited the largest absorbance measurement (1.578  $\pm$  0.133 au), a value significantly higher than both the controls (p = 0.0003) and *S. aureus* samples (p = 0.0004). The greater absorbance of carrier fluid from the *P. aeruginosa* samples is

likely due to pyocyanin, which absorbs at 370 nm.<sup>36</sup> Despite much lower values than *P. aeruginosa*, *S. aureus* samples still showed a significantly greater absorbance (0.459  $\pm$  0.020 au) than the controls (0.403  $\pm$  0.017 au, p = 0.0052).

Analysis of the carrier fluid with HPLC also showed differences among samples colonized with P. aeruginosa, S. aureus, and controls with no bacteria (Figure 5D). As with the carrier fluid from *E. coli*-colonized samples shown in Figure 2C, the same three major peaks of interest were evident again at 11.0 min (Peak i), at 18.0 min (Peak ii), and at 22.5 min (Peak iii) after 24 h. For Peak i, the controls exhibited the largest peak area of 165100 ± 4781 mV·min, while both S. aureus and P. aeruginosa showed this peak decreased to 41304 ± 23190 mV·min and 128567 ± 17617 mV·min, respectively. Furthermore, the peak for P. aeruginosa was noticeably shifted to the later retention time of 11.3 min, which may indicate an alteration to the compound, causing this peak by the metabolic processes of P. aeruginosa or the presence of a new compound eluting at a very similar time. Analysis of Peak ii showed the carrier fluid from the uninoculated controls exhibiting the largest area (96894 ± 2605 mV·min) and S. aureus-colonized samples a decreased area (26202 ± 3361 mV·min), similar to what was observed for E. coli-colonized controls in Figure 2C. Interestingly, the P. aeruginosa samples lacked any peak at this retention time, again suggesting a difference in the way these bacteria were interacting with the compounds in the LB agar. For Peak iii, only carrier fluid from samples colonized with S. aureus showed any signal, with an area of 44700 ± 4042 mV· min or roughly half of the area of the peak observed for E. coli at this retention time. It is interesting to note the differences between S. aureus and P. aeruginosa in the presence and absence of particular peaks in the HPLC spectra. Together with the clear differences in absorbance, these results suggest promise for the vascularized polymer system in providing methods to not only detect the presence of bacteria but also provide information that may lead to their identification.

#### CONCLUSIONS

In this work, we develop and test a new method of detecting surface bacterial growth at buried interfaces using vascularized polymers. Inspired by natural vascular networks in plants and animals that allow for diffusion and long-range transport of signal molecules, we created an empty channel network in a permeable polymer matrix and filled it with a carrier fluid. A layer of E. coli was then added to one side to simulate a contaminated buried interface. After 24 h of bacterial growth, significant differences in the conductivity, absorbance, and HPLC spectra of carrier fluid sampled from the vascular network were clear between E. coli-inoculated samples and controls without bacteria. Tracking changes in the carrier fluid at time points between 0 and 48 h revealed changes in all three measurement methods that coincided with the lag-exponentialstationary growth curve of these organisms. A 2D finite element model of the vascularized polymer system using established equations for bacterial compound production and utilization was employed to model the changes observed in the HPLC spectra. The results showed a very close match between the experimental results and theoretical predictions, suggesting that the system can be accurately modeled. Clinically relevant bacterial strains Staphylococcus aureus and Pseudomonas aeruginosa were also tested and showed clear differences in the conductivity, absorbance, and HPLC peaks in the carrier fluid compared to uninoculated controls. Importantly,

however, notable differences between the results for these two species were also observed, suggesting that it may be possible to distinguish different microorganisms using this method. Together, our results show that vascularized polymers could be a possible solution for surface bacterial detection at buried interfaces such as underground water distribution networks where standard measurement techniques are difficult to perform.

#### AUTHOR INFORMATION

#### **Corresponding Author**

Caitlin Howell — Department of Chemical and Biomedical Engineering and Graduate School of Biomedical Science and Engineering, University of Maine, Orono, Maine 04469, United States; orcid.org/0000-0002-9345-6642; Email: caitlin.howell@maine.edu

#### **Authors**

Brandon Dixon – Department of Chemical and Biomedical Engineering, University of Maine, Orono, Maine 04469, United States

Chenxi Sui – Thomas Lord Department of Mechanical Engineering and Material Science, Duke University, Durham, North Carolina 27708, United States

Anna Briley – Department of Chemical and Biomedical Engineering, University of Maine, Orono, Maine 04469, United States

Po-Chun Hsu — Thomas Lord Department of Mechanical Engineering and Material Science, Duke University, Durham, North Carolina 27708, United States; Pritzker School of Molecular Engineering, University of Chicago, Chicago, Illinois 60637, United States; ⊚ orcid.org/0000-0002-6509-9377

Complete contact information is available at: https://pubs.acs.org/10.1021/acsabm.2c00837

#### **Author Contributions**

The manuscript was written through contributions of all authors.

# **Funding**

The funding for this research was made possible in part by the University of Maine Department of Chemical and Biomedical Engineering. This material is based upon work supported by the National Science Foundation under Grant No. 1939710 and by the National Institute of Diabetes and Digestive and Kidney Diseases of the National Institutes of Health under award number R01DK12880.

#### Notes

The authors declare no competing financial interest.

## ACKNOWLEDGMENTS

The authors thank Dr. Indira Silwal for HPLC technical support as well as Amy Luce and the Forest Bioproducts Research Institute for HPLC instrument time.

#### ABBREVIATIONS

UV-vis, ultraviolet-visible; HPLC, high-performance liquid chromatography; SFG-VS, sum-frequency generation vibrational spectroscopy; OD, optical density; a.u., absorbance units

#### REFERENCES

- (1) Flores-Mireles, A.; Hreha, T. N.; Hunstad, D. A. Pathophysiology, Treatment, and Prevention of Catheter-Associated Urinary Tract Infection. *Top. Spinal Cord Inj. Rehabil.* **2019**, 25 (3), 228–240.
- (2) Filipiak, W.; Sponring, A.; Baur, M. M.; Filipiak, A.; Ager, C.; Wiesenhofer, H.; Nagl, M.; Troppmair, J.; Amann, A. Molecular Analysis of Volatile Metabolites Released Specifically by Staphylococcus Aureus and Pseudomonas Aeruginosa. *BMC Microbiol.* **2012**, *12* (1), 1–16.
- (3) Puig-Verdié, L.; Alentorn-Geli, E.; González-Cuevas, A.; Sorlí, L.; Salvadó, M.; Alier, A.; Pelfort, X.; Portillo, M. E.; Horcajada, J. P. Implant Sonication Increases the Diagnostic Accuracy of Infection in Patients with Delayed, but Not Early, Orthopaedic Implant Failure. *J. Bone It. Surg.* **2013**, *95 B* (2), 244–249.
- (4) Makris, K. C.; Andra, S. S.; Botsaris, G. Pipe Scales and Biofilms in Drinking-Water Distribution Systems: Undermining Finished Water Quality. *Crit. Rev. Environ. Sci. Technol.* **2014**, 44 (13), 1477–1523.
- (5) Juhna, T.; Birzniece, D.; Larsson, S.; Zulenkovs, D.; Sharipo, A.; Azevedo, N. F.; Ménard-Szczebara, F.; Castagnet, S.; Féliers, C.; Keevil, C. W. Detection of Escherichia Coli in Biofilms from Pipe Samples and Coupons in Drinking Water Distribution Networks. *Appl. Environ. Microbiol.* **2007**, *73* (22), 7456–7464.
- (6) Sahoo, D.; Bhatt, M.; Jena, S.; Dash, D.; Chayani, N. Study of Biofilm in Bacteria from Water Pipelines. *J. Clin. Diagnostic Res.* **2015**, 9 (3), 9–11.
- (7) Momba, M. N. B.; Makala, N. Comparing the Effect of Various Pipe Materials on Biofilm Formation in Chlorinated and Combined Chlorine-Chloraminated Water Systems. *Water SA* **2004**, 30 (2), 175–182.
- (8) Szewzyk, U.; Szewzyk, R.; Manz, W.; Schleifer, K. H. Microbiogical Safety of Drinking Water. *Annu. Rev. Microbiol.* **2000**, 54, 81–127.
- (9) Peltola, M.; Kanto Öqvist, C.; Ekman, J.; Kosonen, M.; Jokela, S.; Kolari, M.; Korhonen, P.; Salkinoja-Salonen, M. Quantitative Contributions of Bacteria and of Deinococcus Geothermalis to Deposits and Slimes in Paper Industry. *J. Ind. Microbiol. Biotechnol.* **2008**, *35* (12), 1651–1657.
- (10) Marcato-Romain, C. E.; Pechaud, Y.; Paul, E.; Girbal-Neuhauser, E.; Dossat-Létisse, V. Removal of Microbial Multi-Species Biofilms from the Paper Industry by Enzymatic Treatments. *Biofouling* **2012**, 28 (3), 305–314.
- (11) Llor, C.; Bjerrum, L. Antimicrobial Resistance: Risk Associated with Antibiotic Overuse and Initiatives to Reduce the Problem. *Ther. Adv. drug Saf.* **2014**, *5* (6), 229–241.
- (12) Wistrand-Yuen, E.; Knopp, M.; Hjort, K.; Koskiniemi, S.; Berg, O. G.; Andersson, D. I. Evolution of High-Level Resistance during Low-Level Antibiotic Exposure. *Nat. Commun.* **2018**, *9* (1), 1599.
- (13) CDC. AMR Challenge. https://www.cdc.gov/drugresistance/intl-activities/amr-challenge.html. Accessed March 16th, 2022.
- (14) ISO 18593:2018. Microbiology of the Food Chain Horizontal Methods for Surface Sampling; 2018.
- (15) Jansson, L.; Akel, Y.; Eriksson, R.; Lavander, M.; Hedman, J. Impact of Swab Material on Microbial Surface Sampling. *J. Microbiol. Methods* **2020**, *176*, 106006.
- (16) Probst, A.; Facius, R.; Wirth, R.; Moissl-Eichinger, C. Validation of a Nylon-Flocked-Swab Protocol for Efficient Recovery of Bacterial Spores from Smooth and Rough Surfaces. *Appl. Environ. Microbiol.* **2010**, *76* (15), 5148–5158.
- (17) Yamaguchi, N.; Ishidoshiro, A.; Yoshida, Y.; Saika, T.; Senda, S.; Nasu, M. Development of an Adhesive Sheet for Direct Counting of Bacteria on Solid Surfaces. *J. Microbiol. Methods* **2003**, *53* (3), 405–410
- (18) Zangerl, P.; Matlschweiger, C.; Dillinger, K.; Eliskases-Lechner, F. Survival of Listeria Monocytogenes after Cleaning and Sanitation of Wooden Shelves Used for Cheese Ripening. *Eur. J. Wood Wood Prod.* **2010**, *68* (4), 415–419.

- (19) Guo, W.; Lu, T.; Gandhi, Z.; Chen, Z. Probing Orientations and Conformations of Peptides and Proteins at Buried Interfaces. *J. Phys. Chem. Lett.* **2021**, *12*, 10144–10155.
- (20) Chen, Z.; Shen, Y. R.; Somorjai, G. A. Studies of Polymer Surfaces by Sum Frequency Generation Spectroscopy. *Annu. Rev. Phys. Chem.* **2002**, *53*, 437–465.
- (21) Howell, C.; Maul, R.; Wenzel, W.; Koelsch, P. Interactions of Hydrophobic and Hydrophilic Self-Assembled Monolayers with Water as Probed by Sum-Frequency-Generation Spectroscopy. *Chem. Phys. Lett.* **2010**, 494 (4–6), 193.
- (22) Howell, C.; Schmidt, R.; Kurz, V.; Koelsch, P. Sum-Frequency-Generation Spectroscopy of DNA Films in Air and Aqueous Environments. *Biointerphases* **2008**, *3* (3), FC47.
- (23) Wang, J.; Woodcock, S. E.; Buck, S. M.; Chen, C.; Chen, Z. Different Surface-Restructuring Behaviors of Poly(Methacrylate)s Detected by SFG in Water [14]. *J. Am. Chem. Soc.* **2001**, *123* (38), 9470–9471.
- (24) Clarke, M. L.; Chen, C.; Wang, J.; Chen, Z. Molecular Level Structures of Poly(n-Alkyl Methacrylate)s with Different Side Chain Lengths at the Polymer/Air and Polymer/Water Interfaces. *Langmuir* **2006**, 22 (21), 8800–8806.
- (25) Sierra, C.; Elvira, L.; García, J. L.; Resa, P.; Galán, B. Monitoring Escherichia Coli Growth in M63 Media by Ultrasonic Noninvasive Methods and Correlation with Spectrophotometric and HPLC Techniques. *Appl. Microbiol. Biotechnol.* **2010**, *85* (3), 813–821
- (26) Guerrant, G. O.; Lambert, M. A.; Moss, C. W. Analysis of Short-Chain Acids from Anaerobic Bacteria by High-Performance Liquid Chromatography. *J. Clin. Microbiol.* **1982**, *16* (2), 355–360.
- (27) Tweeddale, H.; Notley-Mcrobb, L.; Ferenci, T. Effect of Slow Growth on Metabolism of Escherichia Coli, as Revealed by Global Metabolite Pool ('metabolome') Analysis. *J. Bacteriol.* **1998**, *180* (19), 5109–5116.
- (28) Van Der Hooft, J. J. J.; Goldstone, R. J.; Harris, S.; Burgess, K. E. V.; Smith, D. G. E. Substantial Extracellular Metabolic Differences Found between Phylogenetically Closely Related Probiotic and Pathogenic Strains of Escherichia Coli. *Front. Microbiol.* **2019**, *10* (FEB), 252.
- (29) Webster, M. S.; Cooper, J. S.; Chow, E.; Hubble, L. J.; Sosa-Pintos, A.; Wieczorek, L.; Raguse, B. Detection of Bacterial Metabolites for the Discrimination of Bacteria Utilizing Gold Nanoparticle Chemiresistor Sensors. *Sensors Actuators, B Chem.* **2015**, 220, 895–902.
- (30) Desmarais, S. M.; De Pedro, M. A.; Cava, F.; Huang, K. C. Peptidoglycan at Its Peaks: How Chromatographic Analyses Can Reveal Bacterial Cell Wall Structure and Assembly. *Mol. Microbiol.* **2013**, *89* (1), 1–13.
- (31) Bennett, B. D.; Kimball, E. H.; Gao, M.; Osterhout, R.; Van Dien, S. J.; Rabinowitz, J. D. Absolute Metabolite Concentrations and Implied Enzyme Active Site Occupancy in Escherichia Coli. *Nat. Chem. Biol.* **2009**, *5* (8), 593–599.
- (32) Pavlova, E.; Pesheva, M.; Savov, V. Biomass Conductivity Estimation of Escherichia Coli. *Biotechnol. Biotechnol. Equip.* **2003**, *17* (1), 153–156.
- (33) Martin, J. D.; Werner, B. G.; Hotchkiss, J. H. Effects of Carbon Dioxide on Bacterial Growth Parameters in Milk as Measured by Conductivity. *J. Dairy Sci.* **2003**, *86* (6), 1932–1940.
- (34) Guo, Y.; Liu, C.; Ye, R.; Duan, Q. Advances on Water Quality Detection by Uv-Vis Spectroscopy. *Appl. Sci.* **2020**, *10* (19), 6874.
- (35) Moore, N.; Flaws, M. Introduction: Pseudomonas Aeruginosa. Clinial Lab. Sci. **2011**, 24, 41.
- (36) Hamad, M. N. F.; Marrez, D. A.; El-Sherbieny, S. M. R. Toxicity Evaluation and Antimicrobial Activity of Purified Pyocyanin from Pseudomonas Aeruginosa. *Biointerface Res. Appl. Chem.* **2020**, *10* (6), 6974–6990.
- (37) Lacombe, B.; Achard, P. Long-Distance Transport of Phytohormones through the Plant Vascular System. *Curr. Opin. Plant Biol.* **2016**, 34, 1–8.

- (38) Raven, J. A. Evolution and Palaeophysiology of the Vascular System and Other Means of Long-Distance Transport. *Philos. Trans. R. Soc. B Biol. Sci.* **2018**, 373 (1739), 20160497.
- (39) Schilmiller, A. L.; Howe, G. A. Systemic Signaling in the Wound Response. *Curr. Opin. Plant Biol.* **2005**, 8 (4), 369–377.
- (40) Coffigniez, M.; Gremillard, L.; Balvay, S.; Lachambre, J.; Adrien, J.; Boulnat, X. Direct-Ink Writing of Strong and Biocompatible Titanium Scaffolds with Bimodal Interconnected Porosity. *Addit. Manuf.* **2021**, *39*, 101859.
- (41) Xu, C.; Yu, S.; Wu, W.; Liu, Q.; Ren, L. Direct Ink Writing of Fe Bone Implants with Independently Adjustable Structural Porosity and Mechanical Properties. *Addit. Manuf.* **2022**, *51*, 102589.
- (42) Ajdary, R.; Reyes, G.; Kuula, J.; Raussi-Lehto, E.; Mikkola, T. S.; Kankuri, E.; Rojas, O. J. Direct Ink Writing of Biocompatible Nanocellulose and Chitosan Hydrogels for Implant Mesh Matrices. *ACS Polym.* **2022**, *2* (2), 97–107.
- (43) Wu, W.; DeConinck, A.; Lewis, J. A. Omnidirectional Printing of 3D Microvascular Networks. *Adv. Mater.* **2011**, 23 (24), H178–83.
- (44) Howell, C.; Vu, T. L.; Lin, J. J.; Kolle, S.; Juthani, N.; Watson, E.; Weaver, J. C.; Alvarenga, J.; Aizenberg, J. Self-Replenishing Vascularized Fouling-Release Surfaces. *ACS Appl. Mater. Interfaces* **2014**, *6* (15), 13299–13307.
- (45) Hansen, C. J.; Wu, W.; Toohey, K. S.; Sottos, N. R.; White, S. R.; Lewis, J. A. Self-Healing Materials with Interpenetrating Microvascular Networks. *Adv. Mater.* **2009**, *21* (41), 4143–4147.
- (46) Marquis, K.; Chasse, B.; Regan, D. P.; Boutiette, A. L.; Khalil, A.; Howell, C. Vascularized Polymers Spatially Control Bacterial Cells on Surfaces. *Adv. Biosyst.* **2020**, *4* (1), 1900216.
- (47) He, Q.; Wang, Z.; Song, Z.; Cai, S. Bioinspired Design of Vascular Artificial Muscle. Adv. Mater. Technol. 2019, 4 (1), 1800244.
- (48) Kozola, B. D.; Shipton, L. A.; Natrajan, V. K.; Christensen, K. T.; White, S. R. Characterization of Active Cooling and Flow Distribution in Microvascular Polymers. *J. Intell. Mater. Syst. Struct.* **2010**, *21* (12), 1147–1156.
- (49) Luo, X.; Wu, H. C.; Tsao, C. Y.; Cheng, Y.; Betz, J.; Payne, G. F.; Rubloff, G. W.; Bentley, W. E. Biofabrication of Stratified Biofilm Mimics for Observation and Control of Bacterial Signaling. *Biomaterials* **2012**, *33* (20), 5136–5143.
- (50) Ly, K. L.; Hu, P.; Pham, L. H. P.; Luo, X. Flow-Assembled Chitosan Membranes in Microfluidics: Recent Advances and Applications. J. Mater. Chem. B 2021, 9 (15), 3258–3283.
- (51) Li, X.; Jin, J.; Zhang, X.; Xu, F.; Zhong, J.; Yin, Z.; Qi, H.; Wang, Z.; Shuai, J. Quantifying the Optimal Strategy of Population Control of Quorum Sensing Network in Escherichia Coli. *npj Syst. Biol. Appl.* 2021 71 2021, 7 (1), 1–16.
- (52) Williamson, K.; McCarty, P. L. A Model of Substrate Utilization by Bacterial Films. *J. Water Pollut. Control Fed.* **1976**, 48, 9–24.
- (53) Johnston, K. A.; Stabryla, L. M.; Smith, A. M.; Gan, X. Y.; Gilbertson, L. M.; Millstone, J. E. Impacts of Broth Chemistry on Silver Ion Release, Surface Chemistry Composition, and Bacterial Cytotoxicity of Silver Nanoparticles. *Environ. Sci. Nano* **2018**, *5* (2), 304–312.
- (54) Sezonov, G.; Joseleau-Petit, D.; D'Ari, R. Escherichia Coli Physiology in Luria-Bertani Broth. *J. Bacteriol.* **200**7, 189 (23), 8746. (55) Guo, A. C.; Jewison, T.; Wilson, M.; Liu, Y.; Knox, C.;
- Djoumbou, Y.; Lo, P.; Mandal, R.; Krishnamurthy, R.; Wishart, D. S. ECMDB: The E. Coli Metabolome Database. *Nucleic Acids Res.* **2012**, *41* (D1), 625–630.
- (56) Donlan, R. M.; Costerton, J. W. Biofilms: Survival Mechanisms of Clinically Relevant Microorganisms. *Clin. Microbiol. Rev.* **2002**, *15* (2), 167–193.

# **□** Recommended by ACS

# Marine Biofilm Engineered to Produce Current in Response to Small Molecules

Lina J. Bird, Sarah M. Glaven, et al.

MARCH 16, 2023

ACS SYNTHETIC BIOLOGY

READ 🗹

### Solar Thermal Textiles for On-Body Radiative Energy Collection Inspired by Polar Animals

Wesley Viola, Trisha L. Andrew, et al.

APRIL 05, 2023

ACS APPLIED MATERIALS & INTERFACES

READ 🗹

### Microbial-Inspired Surface Patterning for Selective Bacterial Actions for Enhanced Performance in Microbial Fuel Cells

Babu Indira Bijimol, Sheik Muhammadhu Aboobakar Shibli, et al.

OCTOBER 27, 2022

ACS APPLIED BIO MATERIALS

READ

# Individual-Based Modeling of Spatial Dynamics of Chemotactic Microbial Populations

Congjian Ni and Ting Lu

NOVEMBER 06, 2022

ACS SYNTHETIC BIOLOGY

READ 🗹

Get More Suggestions >